

Article

Abrasive Surface Finishing on SLM 316L Parts Fabricated with Recycled Powder

Jakub Mesicek , Quoc-Phu Ma * , Jiri Hajnys , Jan Zelinka, Marek Pagac , Jana Petru  and Ondrej Mizera

Department of Machining, Assembly and Engineering Metrology, Faculty of Mechanical Engineering, VSB-Technical University of Ostrava, 70833 Ostrava, Czech Republic; jakub.mesicek@vsb.cz (J.M.); jiri.hajnys@vsb.cz (J.H.); jan.zelinka@vsb.cz (J.Z.); marek.pagac@vsb.cz (M.P.); jana.petru@vsb.cz (J.P.); ondrej.mizera@vsb.cz (O.M.)

* Correspondence: phu.ma.quoc@vsb.cz; Tel.: +420-607326979

Abstract: Improving the surface roughness quality of 3D printed components, especially metallic ones, which are fabricated from the selective laser melting (SLM) method, has drawn enormous attention from the research community. It should be noted that various studies on this topic have reported that precise surface roughness results can be obtained with various techniques that are indeed not cost-effective. Differing itself from these studies, this manuscript investigates an economical solution for fabricating and surface treating SLM components. Specifically, the inspected specimens were printed with recycled 316L stainless steel powder and treated solely with two abrasive surface finishing methods. In the manuscript, two scanning strategies namely meander and stripes, and three types of surfaces were investigated. Subsequently, their 2D and 3D surface roughness results were elaborated. After the proposed herein abrasive treatment, 3D surface roughness arithmetical mean height of a surface (S_a) value of $0.9\ \mu\text{m}$ can be achieved.

Keywords: selective laser melting (SLM); surface roughness; abrasive surface finishing; stainless steel; 316L; recycled powder



Citation: Mesicek, J.; Ma, Q.-P.; Hajnys, J.; Zelinka, J.; Pagac, M.; Petru, J.; Mizera, O. Abrasive Surface Finishing on SLM 316L Parts Fabricated with Recycled Powder. *Appl. Sci.* **2021**, *11*, 2869. <https://doi.org/10.3390/app11062869>

Academic Editor: Guijun Bi

Received: 23 February 2021

Accepted: 19 March 2021

Published: 23 March 2021

Publisher's Note: MDPI stays neutral with regard to jurisdictional claims in published maps and institutional affiliations.



Copyright: © 2021 by the authors. Licensee MDPI, Basel, Switzerland. This article is an open access article distributed under the terms and conditions of the Creative Commons Attribution (CC BY) license (<https://creativecommons.org/licenses/by/4.0/>).

1. Introduction

3D printing technology has enabled designers to fabricate parts that are functional, lighter, and remarkably more complex from various materials [1–3]. Remarkably, for metallic parts fabricated with the selective laser melting (SLM) method, the mechanical properties are higher in comparison with traditionally produced ones [4,5]. Specifically, for SLM technology, it has been advanced so that it can operate with several common alloys utilized in the aerospace, biomedical, and automotive industries [6–9]. Nevertheless, an obvious drawback of 3D printed parts, in general, and SLM parts, in particular, is the large surface roughness caused by the nature of the fabricating process as investigated in [10–13]. Specifically, the surface roughness of SLM parts is mainly influenced by different factors, such as the laser power, laser speed, scanning strategies, position and direction of the parts in the building chamber, direction and flow rate of the inert gas flow, and powder characteristics [8,14–16]. The arithmetic mean high of a line (R_a) of SLM parts could range from 5 up to 50 μm , and is primarily found below 20 μm as in [11,17,18]. Subsequently, without undergoing any post surface finishing, the SLM parts cannot satisfy the requirements of R_a being below 0.8 μm as for machine components and below 1 μm as for dental implants [19].

To achieve the desired surface roughness, as previously mentioned, SLM parts must then undergo the traditional computer numerical control (CNC) machining process [20]. The two fabricating processes indeed have been combined into a so-called hybrid additive-subtractive manufacturing (HASM) process, where adding and subtracting material from a fabricated component are realized simultaneously in one machine [21,22]. However, due to the restriction of the tool path when finish machining a 3D printed part, several alternative

post-processes have been investigated, such as blasting, grinding, laser/electromechanical polishing, shot/ultrasonic peening, etc., as summarized in [23]. Among the most effective techniques is the surface mechanical attrition treatment (SMAT), investigated in [23], where the surfaces of the SLM part were bombarded with steel balls vibrating at 40 Hz in 10 min to reduce the Ra from 15 to 1.8 μm , and longer SMAT time can deliver surface roughness below 0.5 μm . Besides, in [24], ultrasonic peening reduces the Ra from 10.6 to 1.3 μm . Utilizing the dry mechanical-electrochemical polishing (DMECP) technique, [25] led to reducing the Ra to the lowest 0.75 μm . Last but not least, in [19], laser polishing was reported to deliver Sa, the 3D extension of Ra, below 0.51 μm .

There have been several studies on different surface treating methods on SLM parts printed from various materials such as steel, titanium, Inconel, and their alloys, etc. Nevertheless, these aforementioned techniques and material usage require heavy investment in the facilities, which may not be applicable for a majority of entities. Thus, in this case study, SLM stainless steel 316L specimens fabricated with recycled powder were examined. They were treated solely with the mechanical abrasive finishing methods aiming at finding a more affordable solution as an alternative for the aforementioned surface treating methods. Specifically, a combination of blasting and tumbling was investigated in this manuscript. In blasting, surface imperfections are removed by streamlines of media being shot directly to the surface of the components [26]. Additionally, in tumbling, components are tumbled in different solid media added for deburring, surface smoothing, degreasing, increasing corrosion resistance with the help of chemical (tumbling compound), etc. [27]. Specifically, in this manuscript, the as-built parts underwent sand or steel-ball blasting, then tumbled in three different media being ceramic, plastic, and porcelain, for different pre-specified durations. A special geometry was proposed to fully capture the quality of surfaces of the parts facing four different directions on the rectangular build plate. The surface roughness results and the total duration of each treatment combination were evaluated and compared to find the best combination yielding the smallest surface roughness.

2. Experimental Procedure

2.1. Specimen Design

As aforementioned, a special design was proposed to study the surface quality, as shown below in Figure 1:

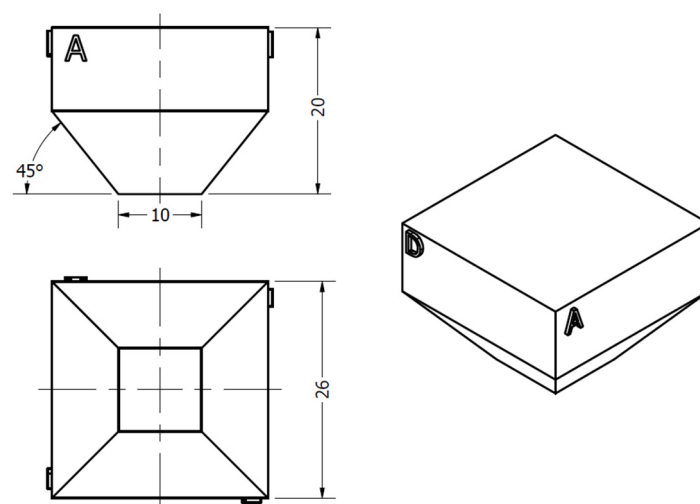


Figure 1. Geometry under study.

The four faces of the design were marked with symbols A, B, C, D for classification. Besides, to assess the “staircase” effect caused by the angled geometry, which is critical to the surface roughness of 3D printed specimens, [19], the inverted truncated pyramid feature was introduced at the bottom of the design. The specimens were printed with

two different scanning strategies, namely meander and stripes. There were in total 16 specimens divided into two packs with regard to the scanning strategies.

2.2. Recycled Powder Characteristics

The machine AM400 from Renishaw with 400 W optical system (pulsed laser) and beam diameter of 70 μm was deployed to print the specimens with recycled stainless steel 316 L powder. The scanning electron microscopy (SEM) image and the average size distribution of the utilized 316 L recycled powder are shown in Figures 2 and 3 below. The characteristics of virgin, recycled, and waste stainless steel 316 L powder were discussed in detail in [15].

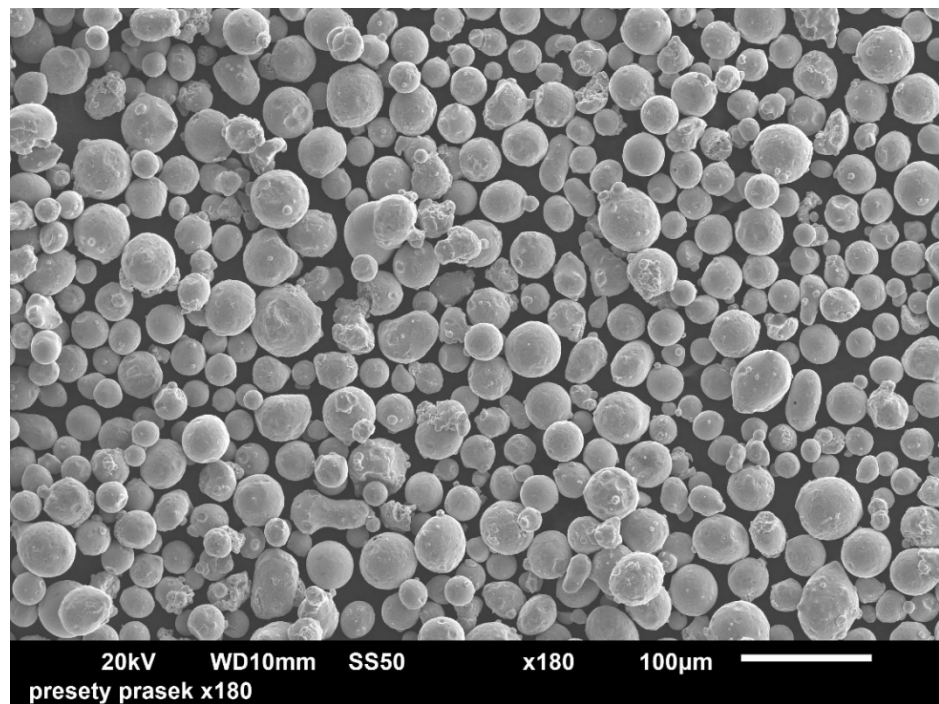


Figure 2. SEM image of the 316 L recycled powder in use.

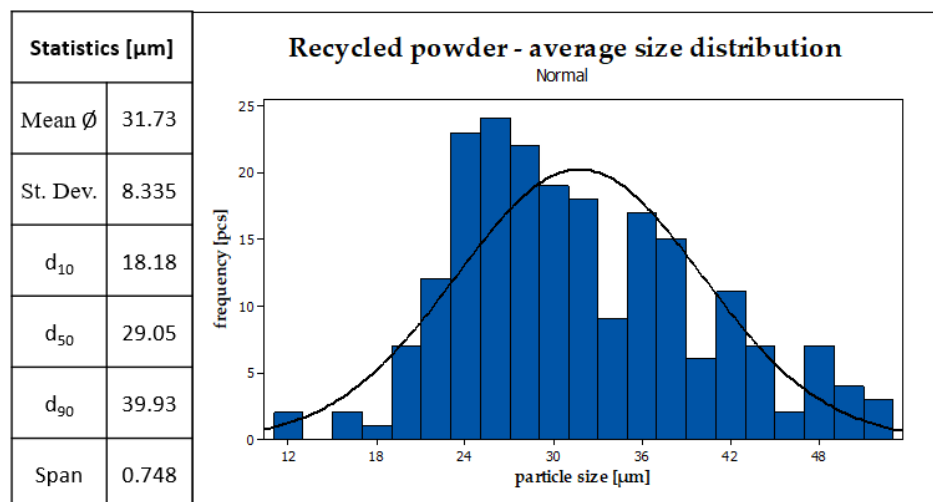


Figure 3. Average size distribution of the 316 L recycled powder in use.

2.3. Machine Setup and Important Notes

The Renishaw company offers two default sets of printing parameters, with laser power of 200 and 400 W. According to our findings, parts fabricated with the default set with laser power of 200 W have better overall mechanical properties [28]. The scanning parameters of this set are listed below in Table 1.

Table 1. Fabrication parameters.

Parameter	Value
Laser power	200 W
Hatch spacing	0.11 mm
Scan speed	650 mm/s
Preheat temperature	Ambient
Layer thickness	50 μm
Increment rotation angle	67°

From Table 1, it can be observed that a parameter, namely increment rotation angle, was set to 67°. With this setup, the coordinate system of each layer is rotated by 67° to ensure that the inside area of the fabricated parts is filled with printed material as much as possible. However, if the rotation point is fixed, the resulting parts would be hollow in the middle. Thus, additional setup to randomize the rotation point for every layer is needed. This principle is explained in Figure 4 below. Notably, the below figure utilizes straight scanned tracks for better illustration, but is applicable as well for meander and stripes strategies.

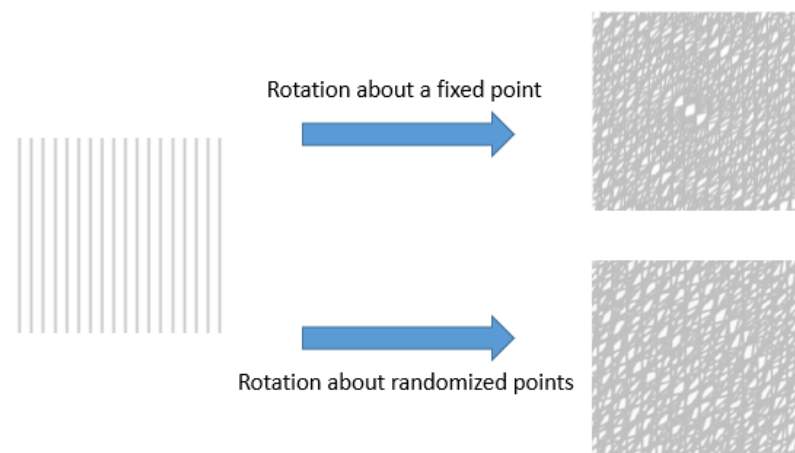


Figure 4. Stacked layers with a fixed rotation point and randomized rotation points.

Additionally, two functions, namely Upskin and Downskin, available in Renishaw machine, were utilized to remelt the exposed surfaces, hiding the scan track patterns, subsequently, improving the smoothness of the specimens. The Upskin effect is illustrated below in Figure 5. It is worth mentioning that the exposed surfaces inherit the pattern of stacked layers, which is depicted in Figure 4, and Figure 5 is simplified for clearer illustration.

The “staircase” effect and the Upskin-treated surfaces are further elaborated on in Figure 6. Remarkably, Figure 6 is valid as well for upside-down direction, as in the case of Downskin function. Differences in Downskin situation lie in the presence of support structures utilized for overhang details.

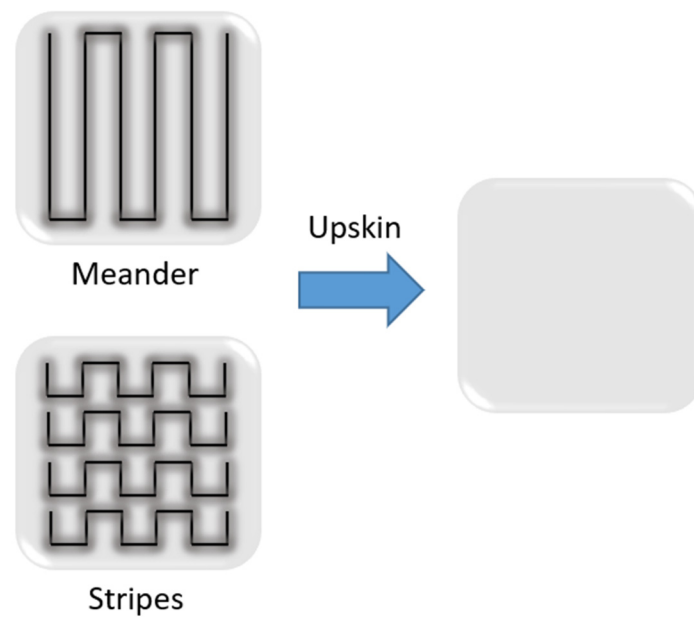


Figure 5. Scan track patterns on the exposed surfaces produced with meander and stripes scanning strategies before and after Upskin treatment.

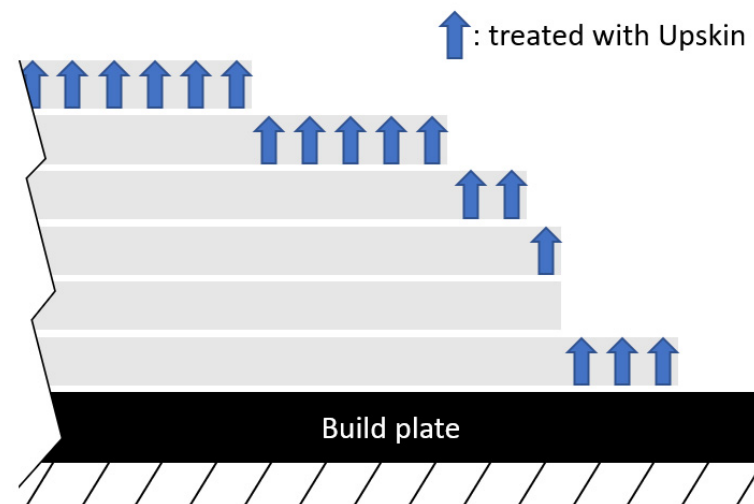


Figure 6. Layers of exposed surfaces treated with Upskin.

2.4. 2D and 3D Surface Roughness Measurement

After fabrication, the as-built specimens were first sandblasted utilizing Cabinet Sandblaster 350 L XH-SBC 350 with either S170 steel medium (grain size from 355 to 425 μm) or F-24 aluminum oxide medium (grain size from 710 to 850 μm) for a recorded duration of 50 s. Subsequently, the specimens were feedforwarded to the tumbler OTEC CF1 \times 32EL for surface finishing within 120, 180, and 240 min, with one of three media being ceramic (DZS 10/10, Otec company, Pforzheim, Germany), plastic (XS 12K, Wather Trowal company, Germany), porcelain (P 2/5 Otec company), and a chemical compound (KFL, Walther Trowal company). The total surface treatment durations of different specimens were recorded.

Eventually, Mitutoyo SJ-210 was employed to measure the 2D surface roughness of nine surfaces (eight sides and one top). Special stands, which were printed from polyethylene terephthalate glycol (PETG) with fused deposition modeling (FDM) technology, were deployed to position the inspected surfaces perpendicular to the measuring needle tip. The needle tip was chosen according to the standard DIN EN ISO 3274 dimensioning of

2 $\mu\text{m}/60^\circ$. The instrument was calibrated so that it can deliver up to 0.001 μm accuracy. Each surface was measured five times, and the mean value of the arithmetical mean high of a line (Ra) and the mean maximum peak to valley of five consecutive sampling lengths of a line (Rz) were then calculated to minimize the measurement error. The projections of the planes of symmetry on the surfaces of the specimen, as can be seen in Figure 1, were used as measuring lines. Because the specimens were printed layer by layer from the truncated bottom to the top, these measuring lines can capture the best the layer nature of the surfaces.

Subsequently, one post-treated specimen with the best 2D roughness from each scanning strategy pack was selected together with their as-built counterparts for 3D surface roughness assessment using the optical microscope Alicona InfiniteFocus 5G (IF MeasureSuite, Alicona Imaging GmbH, Raaba/Graz, Austria). The inspected surfaces were oriented perpendicularly to the microscope axis utilizing as well the designed stands. For 3D roughness measurement, ČSN EN ISO 25,178 -2/-3 standards were followed. The focus variation method was described in the ČSN EN ISO 25,178 -606 standard. Due to the nature of the optical microscope, the Sa and Sz, which are 3D extensions of Ra and Rz to surfaces, were measured once.

The 2D and 3D surface roughness were calculated according to the ČSN EN ISO 4287/4288 standards. Additionally, the normal and macrostructure images of the specimens were presented for a better understanding of the characteristics of the SLM 316L surfaces.

3. Results and Discussion

3.1. 2D Surface Roughness

3.1.1. Average of All Surfaces

This section presents the results of the 2D surface roughness being Ra and Rz. In Table 2 below, different combinations of time and treatments were recorded for two different scanning strategies being meander and stripes. It is worth mentioning that the surface roughness results of all nine sides of the specimens were averaged and rounded to the nearest tenth for generality.

Table 2. Matrix of scanning strategies, treatment time, and corresponding 2D surface roughness results.

Specimen No.	Scanning Strategy		Sandblasting		Tumbling					Total Time [min]	Roughness	
			Corundum	Steel	Ceramic			Plastic	Porcelain		Ra	Rz
	Meander	Stripes	50 [s]	50 [s]	120 [min]	180 [min]	240 [min]	120 [min]	120 [min]	[μm]	[μm]	
1	X									0	11.0	56.6
2	X		X							1	6.6	37.0
3	X		X	X						2	4.9	25.1
4	X				X			X	X	360	3.5	20.5
5	X					X		X	X	420	2.2	15.1
6	X						X	X	X	480	1.8	13.4
7	X		X				X	X	X	481	1.2	9.4
8	X		X	X			X	X	X	482	1.7	10.4
1		X								0	9.5	47.9
2		X	X							1	6.4	35.6
3		X	X	X						2	3.7	20.6
4		X			X			X	X	360	2.9	17.2
5		X				X		X	X	420	1.8	12.5
6		X					X	X	X	480	1.7	12.5
7		X	X				X	X	X	481	1.7	12.3
8		X	X	X			X	X	X	482	0.5	4.4

In Table 2, the specimens can be grouped according to their numbering as follows: as-built (1), sandblasted (2, 3), tumbled (4, 5, 6), combined (7, 8). The sandblasting process took 50 s with two different media being corundum (aluminum oxide) and steel. The tumbling process with plastic, porcelain took 120 min, and with ceramic, 120, 180, 240 min. The total time was recorded and rounded up to min. Averages of surface roughness values for all the sides, Ra and Rz, were calculated. First and foremost, it can be observed that the

Ra values of as-built specimens no. 1 lie within the regular aforementioned range, below 20 μm .

For meander no. 3, after 2 min of sandblasting, Rz was reduced 56% (from 56.6 to 25.1 μm) and Ra 55% (from 11.0 to 4.9 μm). On the other hand, tumbling meander no. 4, which took considerably more time, produced a better roughness reduction of 64% for Rz (from 56.6 to 20.5 μm) and 68% for Ra (from 11.0 to 3.5 μm). Additionally, the roughness value decreased moderately as the time for tumbling with ceramic increased from 120 to 240 min. Last but not least, the two best results are from the combined process. Remarkably, the roughness values for meander no. 8 are slightly higher than those of meander no. 7. This can be due to the imperfection of the manual sandblasting and tumbling process. Eventually, the best result was meander no. 7 with an 83% reduction in Rz (from 56.6 to 9.4 μm) and an 89% reduction in Ra (from 11.0 to 1.2 μm).

As for the stripes strategy, the surface roughness values of as-built stripes no. 1 are slightly lower than those of the meander. Similarly, 2 min of sandblasting vastly reduced the surface roughness of the stripes no. 3, a 57% reduction of Rz (from 47.9 to 20.6 μm) and a 61% reduction of Ra (from 9.5 to 3.7 μm). Solely tumbled stripes no. 4 had a better reduction of roughness, 64% for Rz (from 47.9 to 17.2 μm) and 69% for Ra (from 9.5 to 2.9 μm). However, as the tumbling time increased, it can be observed that there was a slight to no decrease in surface roughness. Subsequently, the best result was stripes no. 8 with 91% reduction in Rz (from 47.9 to 4.4 μm) and 95% reduction in Ra (from 9.5 to 0.5 μm).

3.1.2. Grouped Surfaces

For further inspection into the characteristics of each type of surface, the results were divided into three groups being the vertical sides noted with A, B, C, D (Ra, Rz), the angled sides right below A, B, C, D (RaZk, RzZk), and the top side (RaTop, RzTop). These roughness values were averaged and reported separately according to the scanning strategies in the following Figures 7 and 8, corresponding to the data in Tables 3 and 4.

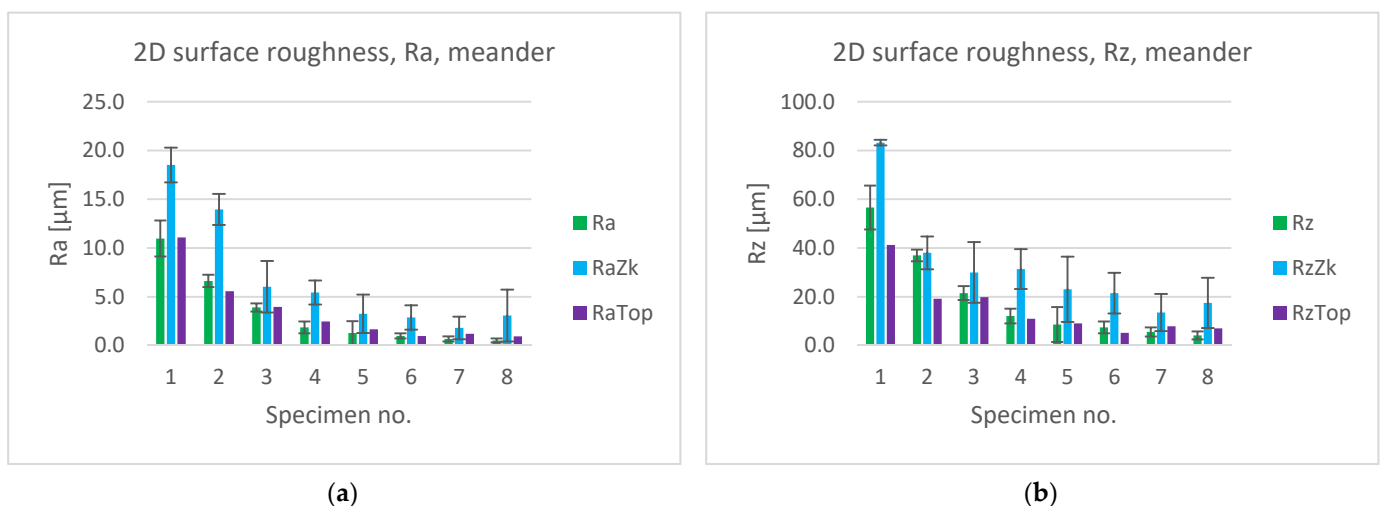


Figure 7. 2D surface roughness results grouped according to the types of surfaces for the meander strategy: (a) Ra, (b) Rz.

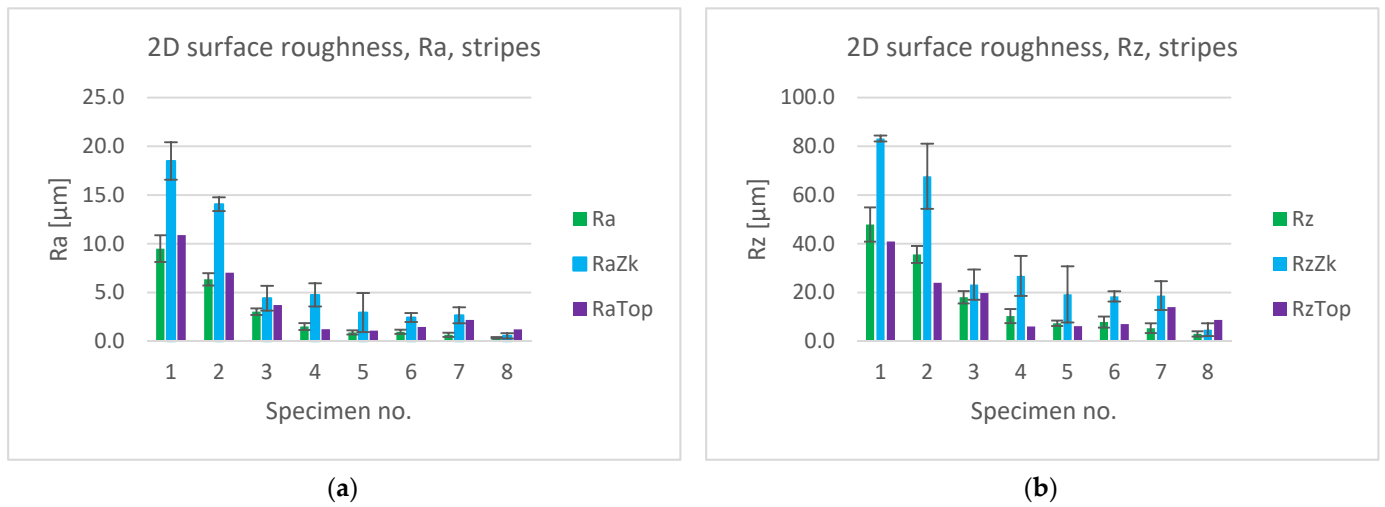


Figure 8. 2D surface roughness results grouped according to the types of surfaces for the stripes strategy: (a) Ra, (b) Rz.

Table 3. 2D surface roughness results, grouped according to the types of surfaces for the meander strategy.

Meander	1	2	3	4	5	6	7	8
Ra [μm]	11.0 ± 1.8	6.6 ± 0.6	3.9 ± 0.4	1.9 ± 0.6	1.3 ± 1.2	1.0 ± 0.3	0.7 ± 0.3	0.5 ± 0.2
RaZk [μm]	18.5 ± 1.8	14.0 ± 1.6	6.0 ± 2.6	5.4 ± 1.2	3.3 ± 2.0	2.9 ± 1.2	1.8 ± 1.2	3.1 ± 2.7
RaTop [μm]	11.1	5.6	4.0	2.5	1.7	1.0	1.2	0.9
Rz [μm]	56.6 ± 9.0	37.0 ± 2.4	21.5 ± 2.8	12.1 ± 3.0	8.6 ± 7.2	7.4 ± 2.4	5.6 ± 1.9	4.1 ± 1.6
RzZk [μm]	83.2 ± 1.1	38.0 ± 6.7	30.0 ± 12.5	31.4 ± 8.2	23.1 ± 13.4	21.5 ± 8.3	13.5 ± 7.6	17.5 ± 10.3
RzTop [μm]	41.3	19.2	19.8	11.0	9.1	5.2	7.9	7.1

Table 4. 2D surface roughness results, grouped according to the types of surfaces for the stripes strategy.

Stripes	1	2	3	4	5	6	7	8
Ra [μm]	9.5 ± 1.4	6.4 ± 0.6	3.0 ± 0.3	1.5 ± 0.4	0.9 ± 0.2	1.0 ± 0.2	0.7 ± 0.2	0.4 ± 0.1
RaZk [μm]	18.5 ± 1.9	14.1 ± 0.7	4.4 ± 1.3	4.8 ± 1.2	2.9 ± 2.0	2.4 ± 0.5	2.7 ± 0.8	0.6 ± 0.3
RaTop [μm]	10.9	7.0	3.7	1.2	1.1	1.5	2.2	1.2
Rz [μm]	47.9 ± 7.0	35.6 ± 3.5	18.1 ± 2.5	10.3 ± 2.9	7.4 ± 1.1	7.9 ± 2.2	5.4 ± 2.0	3.0 ± 1.1
RzZk [μm]	83.2 ± 1.2	67.7 ± 13.4	23.2 ± 6.2	26.8 ± 8.2	19.2 ± 11.5	18.4 ± 2.1	18.7 ± 5.9	4.8 ± 2.6
RzTop [μm]	40.9	24.0	19.8	6.1	6.2	7.1	14.0	8.7

One of the obvious traits from the two figures is that the surface roughness of the angled sides (RaZk, RzZk), in as-built specimens no. 1, is almost double the other two (Ra, Rz and RaTop, RzTop). This is because of the “staircase” effect caused by one layer not being wholly supported by preceding layers. In contrast, as the vertical sides and the top side are built with layers that are fully supported, their surface roughness is remarkably better.

Additionally, as previously drawn, 2 min of sandblasting can significantly reduce the surface roughness from specimens no. 1 to specimens no. 3. Nevertheless, for better surface finishing, tumbling, or a combination of the two processes should be employed at the cost of treatment time. Specifically, Ra value below $1 \mu\text{m}$ can already be achieved from specimens no. 6 for meander and specimen no. 5 for stripes.

3.2. 3D Surface Roughness

From the above results, the best post-treated specimens together with their as-built counterparts of the two types of scanning strategy were selected for 3D surface roughness evaluation. Subsequently, there were four specimens in total being meander no. 1 and 7, and stripes no. 1 and no. 8. The 3D surface roughness values of those specimens, Sa and

Sz, were averaged and rounded to the nearest tenth, as can be observed in Figure 9 and Table 5.

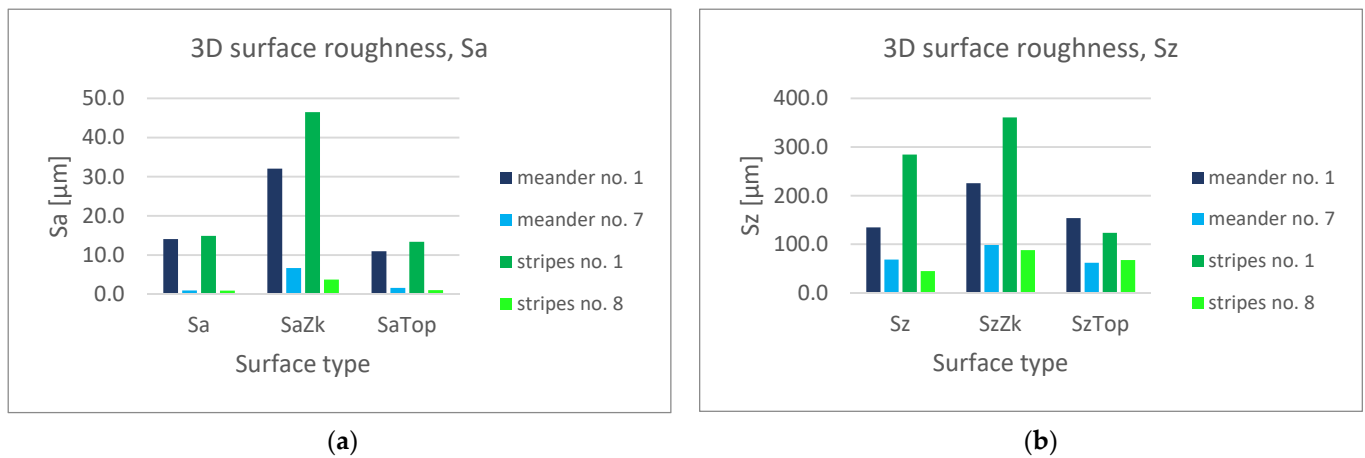


Figure 9. As-built and best 3D surface roughness results grouped according to the types of surfaces for the meander and stripes strategy: (a) Sa, (b) Sz.

Table 5. As-built and best 3D surface roughness results, grouped according to the types of surfaces for the meander and stripes strategy.

Scanning Strategy	No.	Sa [µm]	SaZk [µm]	SaTop [µm]	Sz [µm]	SzZk [µm]	SzTop [µm]
Meander	1	14.1	32.1	10.9	134.6	225.6	153.8
	7	0.9	6.7	1.6	68.4	98.4	62.0
Stripes	1	14.9	46.5	13.4	284.6	361.0	123.6
	8	0.9	3.7	1.0	44.8	87.8	67.5

First of all, it should be noted that the 3D scanned surface results are many-fold higher than the 2D ones. This is due to the fact that 2D scanning is constraint by the height of the scanning tip and scan tracks, thus, fails to thoroughly capture the naturally irregular topographies of the SLM surfaces [14]. In general, at their as-built condition, the meander strategy delivered parts with better surface roughness, meander no. 1 versus stripes no. 1. The angled surfaces had the worst roughness values, as aforementioned. Besides, the roughness values were remarkably reduced after the abrasive finishing process and for the vertical side, Sa was recorded to be reduced by at least 93%, to below 1 µm (0.9 µm) for both meander and stripes. The characteristics of different surface types are depicted in the next subsection.

3.3. Macrostructure

The 3D surface roughness results of the four specimens above can be seen in the macro scale in the below pictures. Take into account that for each measurement, an appropriate height scale was selected to better visualize the maximum height and depth of the surface irregularities.

From Figures 10 and 11 below, it can be observed that the surfaces of the SLM parts are characterized by droplets of melted metallic powder. It can be noticed that in Figure 11(a1), there is a spherical metallic droplet standing out from the others. The reason for this is that the used recycled powder contains unfiltered longitudinally sintered powder particles, as described in [15]. Those pre-melted pieces are accumulated with droplets in this run, subsequently forming the spherical outlier. Besides, the ones with the worst roughness are the angled sides, Figure 10(a2) and Figure 11(a2), with the presence of several peaks and

valleys. As aforementioned, thanks to the Upskin function, the top sides as the as-built condition, Figure 10(a3) and Figure 11(a3), appear to be the smoothest.

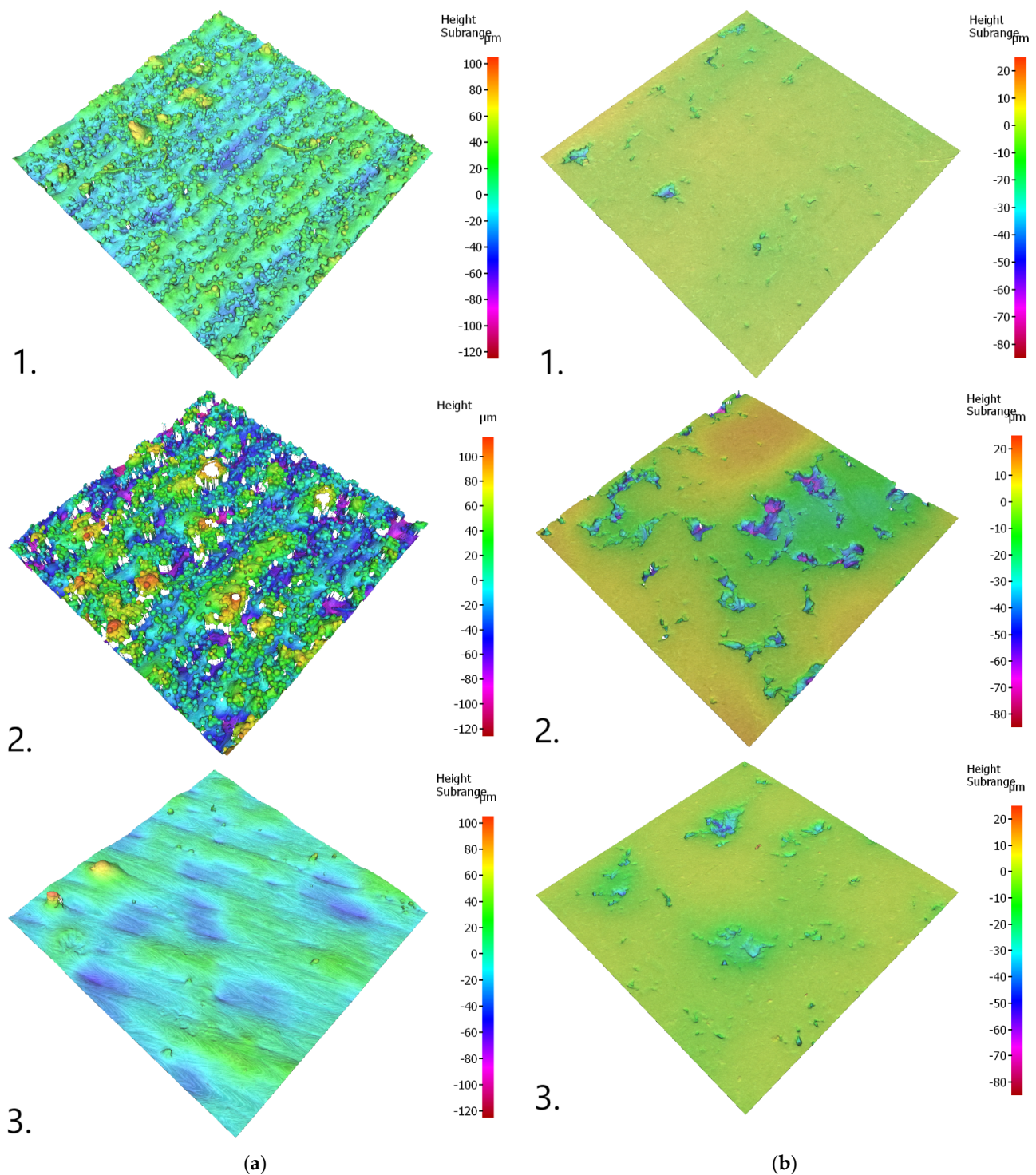


Figure 10. 3D surface roughness with the meander strategy of: (a) as-built, (b) best post-treated. From top to bottom: 1. vertical, 2. angled, and 3. top faces.

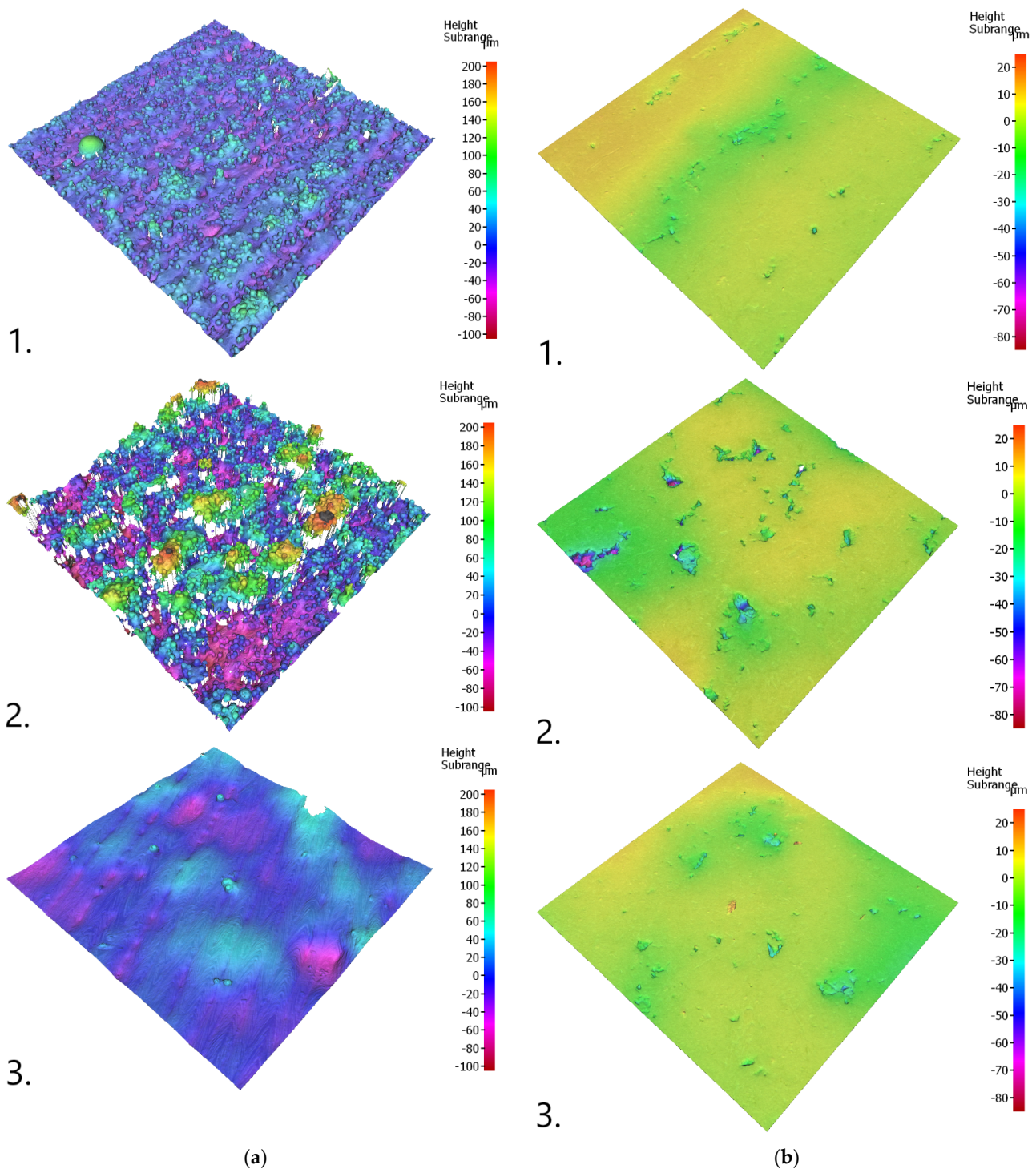


Figure 11. 3D surface roughness with stripes strategy of: (a) as-built, (b) best post-treated. From top to bottom: 1. vertical, 2. angled, and 3. top faces.

One of the obvious traits for post-treated surfaces is the disappearance of the peaks, while valleys remain, which is due to the nature of the abrasive process. After the elimination of the peaks, the depth of the valleys of the angled sides is revealed and is the most severe in comparison with the two other types of surfaces, proving the significant impact of the “staircase” effect on the SLM 316L parts. It is worth noting that the machine built-in functions, such as Upskin and Downskin, can help to improve significantly the surface roughness of the exposed surfaces, which can be obviously observed on the top sides, Figure 10(a3) and Figure 11(a3). Additionally, post-processing can significantly reduce the

waviness of these as-built top sides, from Figure 10(a3–b3) and Figure 11(a3–b3). In general, the peaks and the waviness of the as-built surfaces undergoing the proposed treatment process were notably reduced. Especially for the vertical sides of both scanning strategies, the roughness reduction of Sa down to $0.9\ \mu\text{m}$ was recorded.

3.4. Real Scale Pictures

The reader can refer to Figure 12 below to observe the differences between the as-built specimen and the specimen with the best post-treated 3D surface roughness. It should be noted that only the two specimens from the meander pack were presented. This is because the differences in appearance between them and their stripes counterparts are not visible to the naked eye. Besides, the specimens were numbered differently in this manuscript for better analysis and classification.

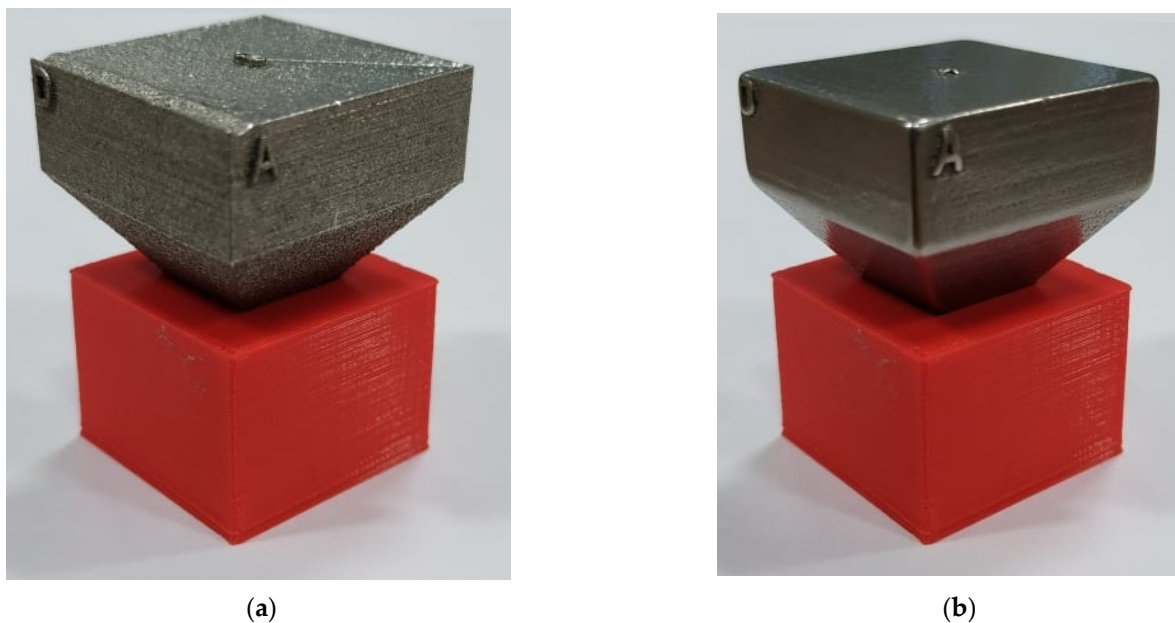


Figure 12. As-built and best post-treated specimens from the meander pack. Metallic parts are the 316L specimens, and red parts are the stands fabricated from PETG using FDM technology: (a) as-built (meander no. 1), (b) best post-treated (meander no. 7).

After the proposed post-treatment, it is obvious that the surfaces became considerably smoother, and all the edges were deburred. According to Table 5, Sa value of down to $0.9\ \mu\text{m}$ can be obtained on A, B, C, D surfaces.

4. Conclusions

To conclude, in the manner of printing materials and facility investment, this manuscript combined two different abrasive surface finishing methods to deliver a cost-effective method to treat the surfaces of SLM 316L parts fabricated from recycled powder. From the obtained results, the characteristics of three different types of surfaces were revealed. The averaged Ra values of as-built specimens fall within the common range of SLM parts as aforementioned in the Introduction, Ra below $20\ \mu\text{m}$ for both meander and stripes. Despite being limited by the height of the scanning tip and the scan tracks, 2D roughness measurement can be utilized for initial screening to choose the best specimens for further time-consuming 3D assessment. From the evaluation, it is obvious that the two best post-treated specimens are meander no. 7 and stripes no. 8. Remarkably, after the proposed abrasive surface treatment, 3D surface roughness Sa and Sz can be reduced significantly, and Sa value of the vertical side surfaces down to $0.9\ \mu\text{m}$ can be obtained. Future studies will combine our findings about the effect of different scanning parameter sets on the surface roughness [29], how effective the hot isostatic pressing is in reducing

the porosity [30], together with post-treatments to optimize not only the surface roughness but also the porosity level and the mechanical properties of the SLM 316L parts. All of these will be realized keeping in mind the cost-effectiveness of the treatment processes.

Author Contributions: Conceptualization, J.M. and J.H.; investigation, J.M., J.H., Q.-P.M., J.Z. and O.M.; writing—original draft preparation, J.M. and Q.-P.M.; writing—review and editing, J.M., Q.-P.M. and J.H.; supervision, M.P. and J.P.; project administration, M.P.; funding acquisition, J.P. All authors have read and agreed to the published version of the manuscript.

Funding: This paper was completed in association with the project Innovative and additive manufacturing technology—new technological solutions for 3D printing of metals and composite materials, reg. no. CZ.02.1.01/0.0/0.0/17_049/0008407 financed by Structural Funds of the European Union and project.

Institutional Review Board Statement: Not applicable.

Informed Consent Statement: Not applicable.

Data Availability Statement: Data has not been uploaded anywhere else.

Conflicts of Interest: The authors declare no conflict of interest.

References

- Hunar, M.; Jancar, L.; Krzikalla, D.; Kaprinay, D.; Srnicek, D. Comprehensive View on Racing Car Upright Design and Manufacturing. *Symmetry* **2020**, *12*, 1020. [[CrossRef](#)]
- Xiao, Z.; Yang, Y.; Xiao, R.; Bai, Y.; Song, C.; Wang, D. Evaluation of topology-optimized lattice structures manufactured via selective laser melting. *Mater. Des.* **2018**, *143*, 27–37. [[CrossRef](#)]
- Marsalek, P.; Sotola, M.; Rybansky, D.; Repa, V.; Halama, R.; Fusek, M.; Prokop, J. Modeling and Testing of Flexible Structures with Selected Planar Patterns Used in Biomedical Applications. *Materials* **2020**, *14*, 140. [[CrossRef](#)] [[PubMed](#)]
- Pagáč, M.; Hajnyš, J.; Petrů, J.; Zlámal, T. Comparison of Hardness of Surface 316L Stainless Steel Made by Additive Technology and Cold Rolling. *Mater. Sci. Forum* **2018**, *919*, 84–91. [[CrossRef](#)]
- Liverani, E.; Toschi, S.; Ceschini, L.; Fortunato, A. Effect of selective laser melting (SLM) process parameters on microstructure and mechanical properties of 316L austenitic stainless steel. *J. Mater. Process. Technol.* **2017**, *249*, 255–263. [[CrossRef](#)]
- Yakout, M.; Elbestawi, M.; Veldhuis, S. Density and mechanical properties in selective laser melting of Invar 36 and stainless steel 316L. *J. Mater. Process. Technol.* **2019**, *266*, 397–420. [[CrossRef](#)]
- Hlinka, J.; Kraus, M.; Hajnyš, J.; Pagac, M.; Petrů, J.; Brytan, Z.; Taňski, T. Complex Corrosion Properties of AISI 316L Steel Prepared by 3D Printing Technology for Possible Implant Applications. *Materials* **2020**, *13*, 1527. [[CrossRef](#)] [[PubMed](#)]
- Chen, Z.; Wu, X.; Tomus, D.; Davies, C. Surface roughness of Selective Laser Melted Ti-6Al-4V alloy components. *Addit. Manuf.* **2018**, *21*, 91–103. [[CrossRef](#)]
- Mohammadian, N.; Turenne, S.; Brailovski, V. Surface finish control of additively-manufactured Inconel 625 components using combined chemical-abrasive flow polishing. *J. Mater. Process. Technol.* **2018**, *252*, 728–738. [[CrossRef](#)]
- Strano, G.; Hao, L.; Everson, R.; Evans, K. Surface roughness analysis, modelling and prediction in selective laser melting. *J. Mater. Process. Technol.* **2013**, *213*, 589–597. [[CrossRef](#)]
- Wang, D.; Liu, Y.; Yang, Y.; Xiao, D. Theoretical and experimental study on surface roughness of 316L stainless steel metal parts obtained through selective laser melting. *Rapid Prototyp. J.* **2016**, *22*, 706–716. [[CrossRef](#)]
- Leary, M. *Surface Roughness Optimisation for Selective Laser Melting (SLM): Accommodating Relevant and Irrelevant Surfaces*; RMIT University, Centre for Additive Manufacturing: Melbourne, VIC, Australia, 2017; pp. 99–118.
- Vayssette, B.; Saintier, N.; Brugger, C.; Elmay, M.; Pessard, E. Surface roughness of Ti-6Al-4V parts obtained by SLM and EBM: Effect on the High Cycle Fatigue life. *Procedia Eng.* **2018**, *213*, 89–97. [[CrossRef](#)]
- Townsend, A.; Senin, N.; Blunt, L.; Leach, R.; Taylor, J. Surface texture metrology for metal additive manufacturing: A review. *Precis. Eng.* **2016**, *46*, 34–47. [[CrossRef](#)]
- Hajnyš, J.; Pagac, M.; Mesicek, J.; Petru, J.; Spalek, F. Research of 316L Metallic Powder for Use in SLM 3D Printing. *Adv. Mater. Sci.* **2020**, *20*, 5–15. [[CrossRef](#)]
- Kozior, T.; Bochnia, J. The Influence of Printing Orientation on Surface Texture Parameters in Powder Bed Fusion Technology with 316L Steel. *Micromachines* **2020**, *11*, 639. [[CrossRef](#)] [[PubMed](#)]
- Yamaguchi, H.; Fergani, O.; Wu, P. Modification using magnetic field-assisted finishing of the surface roughness and residual stress of additively manufactured components. *Cirp Ann.* **2017**, *66*, 305–308. [[CrossRef](#)]
- Yadollahi, A.; Shamsaei, N. Additive manufacturing of fatigue resistant materials: Challenges and opportunities. *Int. J. Fatigue* **2017**, *98*, 14–31. [[CrossRef](#)]
- Tian, Y.; Gora, W.; Cabo, A.; Parimi, L.; Hand, D.; Tammam-Williams, S.; Prangnell, P. Material interactions in laser polishing powder bed additive manufactured Ti6Al4V components. *Addit. Manuf.* **2018**, *20*, 11–22. [[CrossRef](#)]

20. Kaynak, Y.; Kitay, O. Porosity, Surface Quality, Microhardness and Microstructure of Selective Laser Melted 316L Stainless Steel Resulting from Finish Machining. *J. Manuf. Mater. Process.* **2018**, *2*, 36. [[CrossRef](#)]
21. Du, W.; Bai, Q.; Zhang, B. A Novel Method for Additive/Subtractive Hybrid Manufacturing of Metallic Parts. *Procedia Manuf.* **2016**, *5*, 1018–1030. [[CrossRef](#)]
22. Li, L.; Haghighi, A.; Yang, Y. A novel 6-axis hybrid additive-subtractive manufacturing process: Design and case studies. *J. Manuf. Process.* **2018**, *33*, 150–160. [[CrossRef](#)]
23. Sun, Y.; Bailey, R.; Moroz, A. Surface finish and properties enhancement of selective laser melted 316L stainless steel by surface mechanical attrition treatment. *Surf. Coat. Technol.* **2019**, *378*, 124993. [[CrossRef](#)]
24. Zhang, H.; Zhao, J.; Liu, J.; Qin, H.; Ren, Z.; Doll, G.; Dong, Y.; Ye, C. The effects of electrically-assisted ultrasonic nanocrystal surface modification on 3D-printed Ti-6Al-4V alloy. *Addit. Manuf.* **2018**, *22*, 60–68. [[CrossRef](#)]
25. Bai, Y.; Zhao, C.; Yang, J.; Fuh, J.; Lu, W.; Weng, C.; Wang, H. Dry mechanical-electrochemical polishing of selective laser melted 316L stainless steel. *Mater. Des.* **2020**, *193*, 108840. [[CrossRef](#)]
26. Sagbas, B. Post-Processing Effects on Surface Properties of Direct Metal Laser Sintered AlSi10Mg Parts. *Met. Mater. Int.* **2019**, *26*, 143–153. [[CrossRef](#)]
27. Lichovník, J.; Mizera, O.; Sadílek, M.; Čepová, L.; Zelinka, J.; Čep, R. Influence of Tumbling Bodies on Surface Roughness and Geometric Deviations by Additive SLS technology. *Manuf. Technol.* **2020**, *20*, 342–346.
28. Pagac, M.; Hajnys, J.; Petru, J.; ZLaMAL, T.; Sofer, M. The study of mechanical properties stainless steel 316L after production from metal powder with using additive technology and by method selective laser melting. *Int. Conf. Metall. Mater. Conf. Proc.* **2017**, *2017-Jan*, 962–967.
29. Hajnys, J.; Pagac, M.; Kotera, O.; Petru, J.; Scholz, S. Influence of basic process parameters on mechanical and internal properties of 316L steel in SLM process for Renishaw AM400. *MM Sci. J.* **2019**, 2790–2794. [[CrossRef](#)]
30. Cegan, T.; Pagac, M.; Jurica, J.; Skotnicova, K.; Hajnys, J.; Horsak, L.; Soucek, K.; Krpec, P. Effect of Hot Isostatic Pressing on Porosity and Mechanical Properties of 316 L Stainless Steel Prepared by the Selective Laser Melting Method. *Materials* **2020**, *13*, 4377. [[CrossRef](#)]